https://doi.org/10.17221/53/2023-RAE

Study on parameters affecting vibration in height adjustment of a combine harvester header model

*Kittikhun Prasertkan[1], Prathuang Usaborisut[2,] *, Krittatee Jindawong[1], Kiatkong Suwannakij[1], Anusorn Iamrurksiri[1]*

[1]*National Metal and Materials Technology Center (MTEC), Prathumthani, Thailand*
[2]*Department of Agricultural Engineering, Faculty of Engineering at Kamphaengsaen, Kasetsart University, Kamphaengsaen Campus, Nakhonpathom, Thailand*

**Corresponding author: fengptu@ku.ac.th*

Citation: Prasertkan K., Usaborisut P., Jindawong K., Suwannakij K., Iamrurksiri A. (2024): Study on header movement parameters affecting vibration during height adjustment of combine harvester header model. Res. Agr. Eng., 70: 92–103.

Abstract: In Thailand, vibration problems often occur with rice combine harvester automatic header height adjusting systems. This study aimed to identify parameters for reducing the vibration and managing response time for harvesting speed configuration. An experimental combine harvester header model was designed to automatically adjust three parameters: total movement time, time ratio, and final phase distance within vertical movement ranges of 200, 250, or 300 mm. These parameters were controlled using a proportional flow control valve and a professional learning community (PLC) control unit. The results showed that increased time ratio, final phase distance, and total movement time significantly reduced average vibration amplitude. Higher time ratios corresponded to lower vibration amplitude during changing stages but higher amplitude during stopping stages. Vibration amplitudes during starting, changing, and stopping stages ranged from 0.622 to 1.373 mm, 0.042 to 1.097 mm, and 0.132 to 0.902 mm, respectively, for 200, 250, and 300 mm vertical movement distances. To reduce vibration in the first and second wave phases, precise control of start and final speeds through time ratio and total movement time was necessary. Minimizing the time ratio and final phase distance effectively reduced vibration amplitude in the third wave phase.

Keywords: automatic control; rice; vibration amplitude

Thailand is one of the world's major rice producers and exporters, with rice being the country's most important crop and serving as a fundamental staple in people's lives. However, several factors contribute to significant losses during the harvesting process utilising rice combine harvesters. Among these, vibrations from multiple excitation sources emerge as a prominent issue during harvesting. Prolonged and intense vibrations can adversely impact the harvesting efficiency and reliability of the combine harvester (Huang et al. 2019; Tang et al. 2019a; Chen et al. 2020).

Mechanical vibration is recognised to cause structural failures in machinery, leading to fatigue damage in the combine harvester frame (Lai et al. 2018; An et al. 2020). Research by Tang et al. (2019) demonstrated a correlation between the front header's amplitude and the length distribution of the short

Supported by the National Science and Technology Development Agency "Development of the automatic level controlling system of the header of a rice combine harvester" (Project No. P–20–51533).

https://doi.org/10.17221/53/2023-RAE

stalk. With the mean length of the cut stems being 23.60 mm, the up–and–down vibration of the header at 25.36 mm is closely linked to the repeatedly cut stems. This vibration issue becomes particularly critical when harvesting native rice paddy varieties, where the rice paddy grains are more prone to falling (Chinsuwan et al. 2003).

The significance of the header's function in the combine harvester is evident, and the factors causing losses have been well-researched. Vibration during combine harvesting increases grain loss (Lashgari et al. 2008; Ebrahimi et al. 2013; Wang and Su 2021). The header height is the distance between the cutter-bar tip and the ground. Ensuring proper header height during operation is critical. If the header is too high, stubble height increases, leading to grain loss (Glancey 1997; Junsiri and Chinsuwan 2009). Conversely, operating the header at too low a height can cause the header to scratch the ground and result in machine failure (Xie and Alleyne 2014; Ni et al. 2021; Ruan et al. 2022). It has been estimated that approximately 75–80% of harvest losses are caused by improper height adjustment of the header height (Quick and Buchele 1974; Xie et al. 2010; Yang et al. 2022).

Several factors contribute to significant losses to address the vibration challenges in the header during combine harvesting. One such method involves using a perpendicular axis type with a chain–driven cutter bar, which helps reduce vibration in the rice combine harvester. However, exceeding the driver's axial speed of 350 revolutions per minute (rpm) for the header increases vertical vibration (Chuan–Udom 2010). Other strategies include developing the knife driving system to obtain parameters for balance weights, effectively reducing vibration (Fukushima et al. 2012), and installing vibration isolating devices in the chassis frame connection position to minimize vibration (Gao et al. 2017). Many foreign combine harvester companies have developed automatic header height control systems to tackle this long-standing issue. Automatic header height control has been used in the combine harvester to reduce the operator's grain loss and workload while increasing the combine harvester's efficiency (Lopes et al. 2002; Baerdemaeker and Saeys 2013).

Intelligent machines offer the potential to significantly improve the productivity of conventional farming, where farmers manually carry out crop cultivation and management (Xia et al. 2015). Studies have explored various control systems for header height, such as using an ultrasonic sensor as a distance sensor for effective header height control (Zhu et al. 2012), an angle sensor–based adaptive control system for a 5–11 $km \cdot h^{-1}$ harvesting speed range (Yang et al. 2022). Their results showed that the height error in cutting stubble was not more than 2 cm. Yong et al. (2018) studied the height of crops and the header, which were detected using a unilateral infrared reflection device, with the lifting height of the hydraulic cylinder with the displacement sensor and the response speed of the header in rising and falling set at 0.22 and 0.16 $m \cdot s^{-1}$, respectively. The rising and falling of the header were controlled using a fuzzy proportional integral derivative (PID) algorithm and took the crop's actual cutting height as the control objective. The test results showed that the maximum error of the height adjustment was 20 mm, and the error range of the crop height detector was 0–20 mm.

In the quest to minimise vibration-induced losses during header movement, adjusting the vertical movement of the header is crucial in reducing vibration amplitude (Chuan–Udom 2010; Tang et al. 2019b). However, fine–tuning the height of the header with the existing hydraulic control system in Thai combine harvesters poses challenges due to the conventional system's limited response range and improper flow and pressure settings. Therefore, developing an automatic header height system using an electronic directional control valve and a proportional flow control valve is warranted to address vibration management effectively. Thus, this research investigated the parameters involved in reducing the vibration of the header during movement based on the conventional hydraulic system of a Thai combine harvester. The parameters studied were: time ratio, total movement time, and final phase distance with three levels of vertical height movement. The study was carried out on a model of the header of a combine harvester. The working movement parameters were varied to clarify their effects and minimize the header's vibration.

MATERIAL AND METHODS

System design. The design of the header and movement system of a combine harvester used in the study was based on the scaling method for the position, linkage, the length corresponding to a conventional Thai combine header. Figure 1 illustrates a schematic diagram of the combine har-

https://doi.org/10.17221/53/2023-RAE

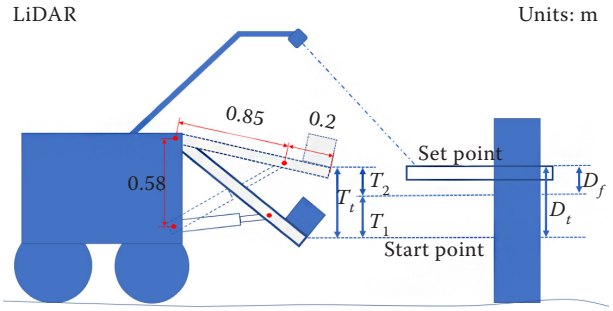

Figure 1. The schematic diagram for adjusting header height
T_t – the total movement time; T_1 – the time of first step movement; T_2 – the time of the final movement distance; D_f – the final phase distance; D_t – the total vertical distance

vester model. With a scaling factor of 0.4, the header comprises a 1.05 m linkage bar jointed to the frame at one end while being supported by a hydraulic rod at 0.85 m and carrying a dead weight at the other end. The hydraulic cylinder is attached to the frame, 0.58 m below the first joint between the frame and the header linkage bar. The height of an object was measured using a LiDAR unit (UST–05LX; Hokuyo Automatic, Japan) installed at the top of the header model. A double-acting hydraulic cylinder adjusted the header height with a proportional flow control valve controlling the movement speed. A linear variable differential transformer sensor between the header and the main frame ensured the system's measuring output when the harvester header height was fine-tuned automatically. A 1.0 Hp power pack unit pack unit powered the header lifting and lowering, set the pressure to 10,000 kPa, and the fixed flow rate of 4.0 L·min^{-1}. A 17.0 kg dead weight was placed 0.2 m away from the tip of the double-acting hydraulic cylinder (bore diameter 30 mm, rod diameter 20 mm, and stroke 380 mm). A triaxial acceleration transducer (AS–10TG; Kyowa Electronic Instruments, Japan) was installed at the bottom end of the header bar. The vibration acceleration signal values of the X and the Z axes were summed as the vector of the vertical vibration acceleration. The vibration analysis software performed fast Fourier transformation (FFT) on the vibration signal to obtain the spectrum of the vibration values (vibration frequency and vibration acceleration). The root mean square (RMS) value of the vibration amplitude was calculated using Equation (1) (Buscarello 1994):

$$D = \frac{0.707 \times A}{(2\pi f)^2} \quad (1)$$

where: D – the vibration amplitude (mm); A – the vibration acceleration (mm·s^{-2}); f – the vibration frequency (Hz).

The header had three movement height levels (200, 250, and 300 mm) corresponding to the adjustment of the header during actual rice harvesting. The standing stubble height was approximately 25–30 cm (Parihar et al. 2023), allowing optimal performance moving between cutting fallen rice and standing rice with high harvest efficiency. The header movement was controlled using two steps to simulate the total height adjustment, as done manually by a combine harvester driver. Therefore, the vertical movement in the current study was determined by two factors: D_t, which represented the total vertical distance (200, 250, or 300 mm), and D_f, which represented the final step movement distance with three fixed vertical distances (50, 70, or 90 mm), as shown in Figure 1. These setting movements resulted in the time parameter needed to define the movement of the header, including time ratio, total movement time, as in Equations (2) and (3), and the speed ratio, as in Equation (4):

$$Ti = \frac{T_1}{T_2} \quad (2)$$

$$Ti = T_1 + T_2 \quad (3)$$

where: T_i – the time ratio; T_1 – the time of first step movement (s); T_2 – the time of the final movement distance (s); T_t – the total movement time (s)

$$Si = \frac{T_2(D_t - D_f)}{D_f \times T_1} \quad (4)$$

where: S_i – the speed ratio; D_t – the total vertical moving distance (mm); D_f – the final phase distance (mm).

Operation principle header adaptive control system. The adaptive header control system's structure is shown in Figure 2. When the adaptive header control system starts, the operator must move the header to the start point to set the zero level. The closed loop of the header control system monitors the real-time header height. The object height value is measured using a LiDAR sensor with a microcontroller control system converted to a voltage signal (0–5V at 0–1 500 mm) and sent to the professional learning community (PLC) controller to adjust the hydraulic actuator speed and header height level. The hydraulic actuator speed is controlled using

https://doi.org/10.17221/53/2023-RAE

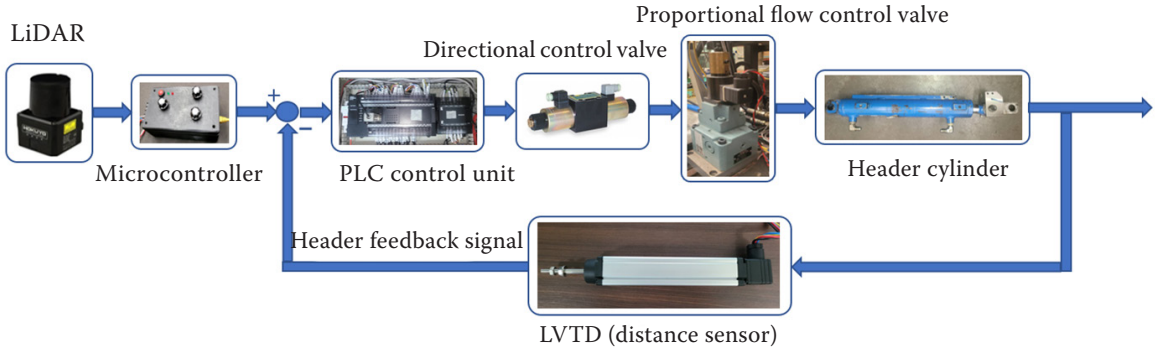

Figure 2. Header adaptive control system structure

PLC – professional learning community; LVTD – linear variable differential transforme

the proportional flow control valve. Figure 3 illustrates the working principle of the header speed control diagram, which includes components such as a pump, relief valve, proportional flow control valve, proportional valve, flow control valve, and hydraulic cylinder. The hydraulic circuit operates at a pressure of 10 000 kPa with a fixed flow rate of 4 L·min^{-1}, The control principle is to generate the corresponding magnetic field by energizing a solenoid coil of the proportional flow control valve to control the speed. Directional and proportional flow control valves control the vertical movement of the header. The amount of voltage signal supplied to the proportional flow control valve is set according to determined parameters, including the total vertical movement (D_t), the final phase distance (D_f), the entire movement time (T_t), and the time ratio (T_i). The movement control process starts with opening the directional and proportional flow control valves by setting the voltage to a pre-determined value. The supplied voltage is changed at the final step moment and set back to 5V in the stopping stage, waiting for the next loop, as shown in Figure 4. A change in direction (rising and falling of the hydraulic cylinder) is generated by energizing the solenoid coil of the direction valve. The feedback of the actual header height is also used as a linear variable differential transformer sensor (distance sensor). All data are sent to the PLC controller in real-time.

Test procedures and instrumentation. The tests were conducted using three levels of total vertical moving distance (200, 250, or 300 mm). For each test, the experiments were carried out based on a factorial statistical design with the three variables being: time ratio (0.75, 1, or 1.5), total movement time (1.5, 2.0, or 2.5 sec), and final phase distance (50, 70, or 90 mm) with three replications. To monitor vibrations during the testing process, a triaxial acceleration transducer (AS–10TG; Kyowa Electronic Instruments, Japan) was securely attached to the bottom end of the header bar. This transducer provided measurements of vibration

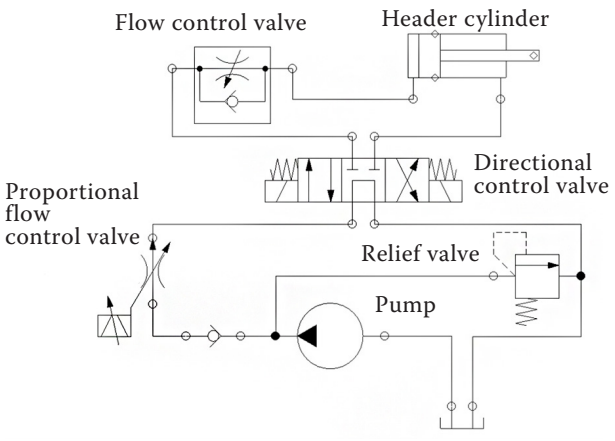

Figure 3. Hydraulic control diagram for header speed

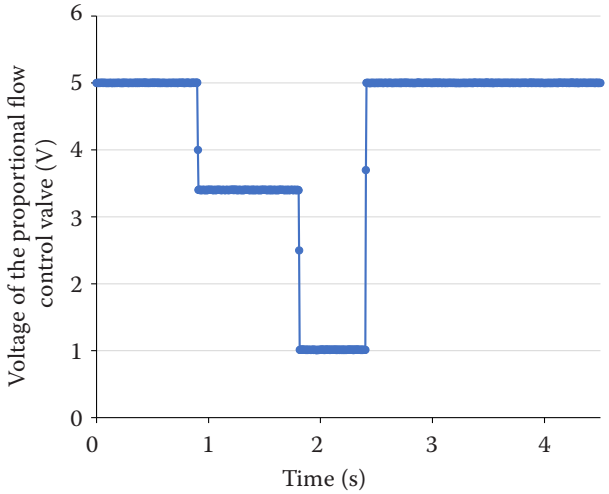

Figure 4. Typically supplied voltage to proportional flow control valve during vertical movement of the header

https://doi.org/10.17221/53/2023-RAE

acceleration along the X and Z axes, which were combined to calculate the vector of vertical vibration acceleration. The obtained data was divided into three distinct phases: the initial phase, the phase during speed change at the final step, and the phase when motion ceased. For each phase, values of the first three vibration waves were extracted to calculate the magnitude of the vibration. The data were then analysed for header vibration by examining the spectrum of the vibration values over the entire movement. This analysis was further divided into the three aforementioned phases to better understand vibration patterns. The evaluation of vibration amplitude specifically focused on the first three waves, which represent periods of high vibration. The average vibration amplitude was determined across the entire range of the total movement time. Duncan's multiple range tests in the results indicated statistical differences at a probability test level of 5%.

Figure 5 shows a schematic diagram of an instrumentation system to measure vibration acceleration. The device consisted of a triaxial acceleration transducer for measuring acceleration, a linear variable differential transformer sensor (distance sensor) for feedback control, a data acquisition card (NI cDAQ–9171: National Instruments, Hungary) for acquiring acceleration and module NI (NI 9237 and NI 9205; National Instruments Hungary) for reading signals at a sampling rate of 400 Hz. All data were stored in the internal memory of the laptop.

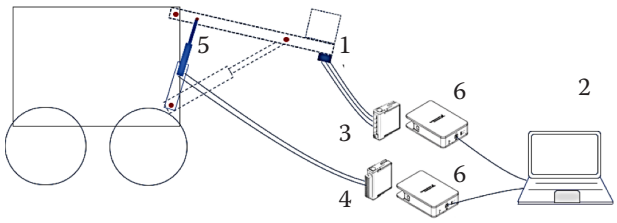

Figure 4. Typically supplied voltage to proportional flow control valve during vertical movement of the header
1 – triaxial acceleration transducer; 2 – laptop; 3 – module NI 9237; 4 – module NI 9205; 5 – linear variable differential transformer sensor; 6 – data acquisition card NI cDAQ-9171

RESULTS AND DISCUSSION

Characteristic of vibration. Figure 6 shows the typical vertical distance during movement in the model of the harvester header. The start time was 0.92 sec with a constant speed that changed at 1.78 sec and stopped at 2.24 sec. This was the result of an experiment under a total movement time (T_t) of 1.5 sec, a time ratio (T_1/T_2) of 0.75, and a final phase distance (D_f) of 50 mm. Figure 7 shows the corresponding vertical speed during the movement of the header. The start speed was 16.67 cm·s^{-1}, and the final speed was 8.33 cm·s^{-1}. There were three–speed changes during moving, causing accelerations of 1 280.8 mm·s^{-2} ($a1$), –740.8 mm·s^{-2} ($a2$), and –585.7 mm·s^{-2} ($a3$) at initial movement, entering the final movement distance, and the stopping stage, respectively. Ac-

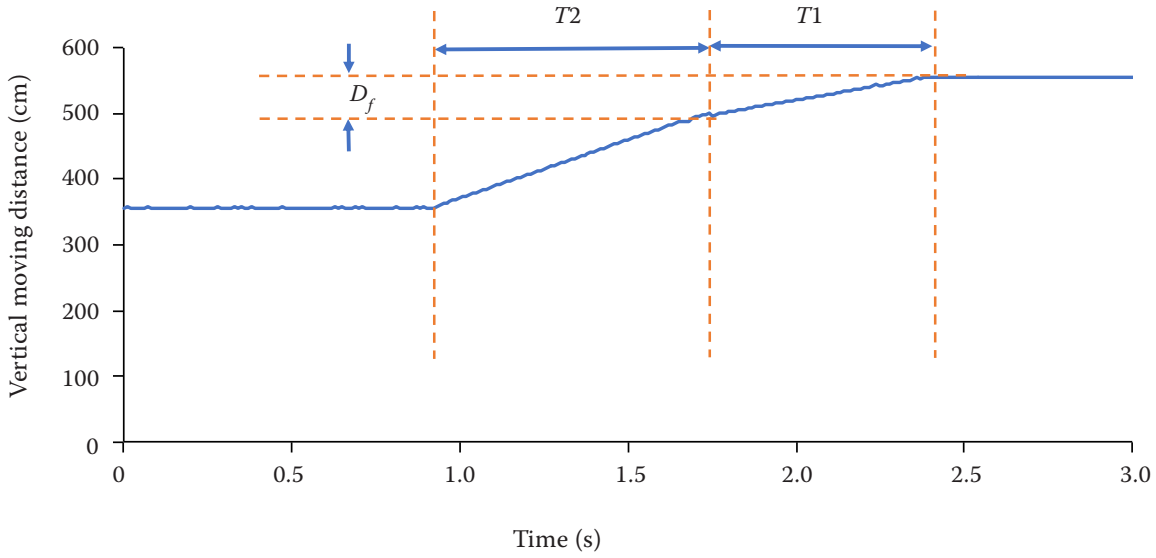

Figure 6. Vertical moving distance during movement of combine harvester header model
T_1 – the time of first step movement; T_2 – the time of the final movement distanc ; D_f – the final phase distance

https://doi.org/10.17221/53/2023-RAE

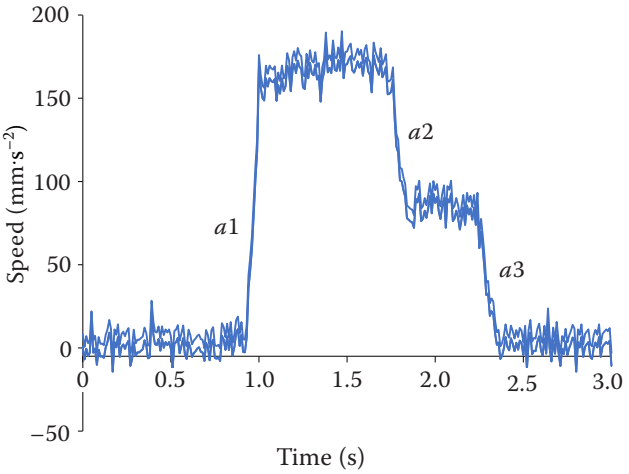

Figure 7. Corresponding vertical speed during movement of the header

*a*1 – the initial movement distance; *a*2 – the final movement distance; *a*3– the stopping stage

cording to all test results, the acceleration and deceleration values increases were related to the difference in changing speed during movement.

Power spectrum of vibration. The moving pattern of the header with two steps generated three wave phases of vibration: the first at the start, the second when getting to the final movement distance, and the third at the stop, as shown in Figure 8A. The first wave had the highest vibration amplitude, followed by the second and third, respectively. Typical results are shown in Figure 8, where the vibration occurred during the vertical movement of 300 mm. The final movement distance likely affected the magnitude of the vertical acceleration. The second and third waves differed under different final movement

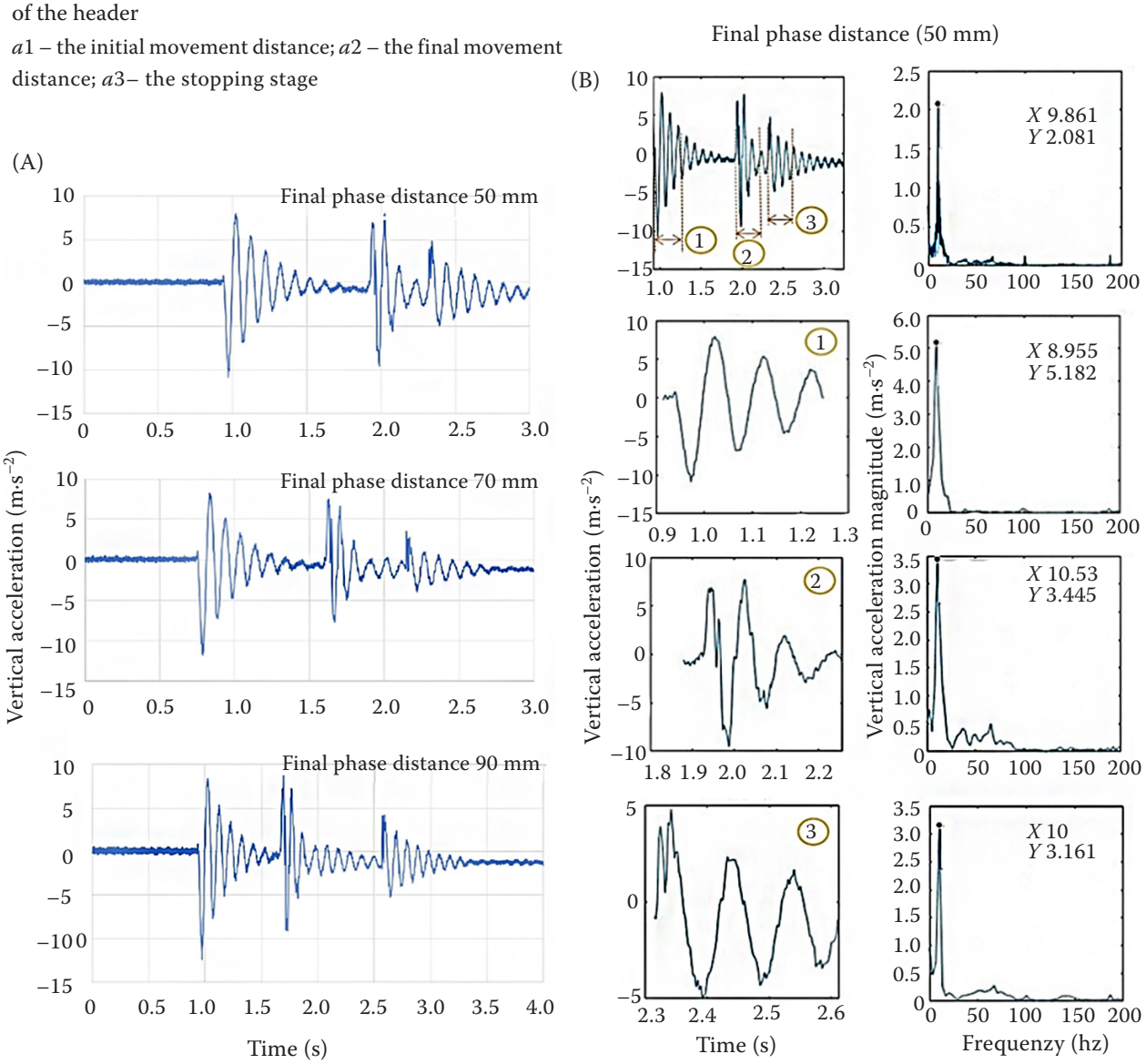

Figure 8. (A) Vertical acceleration at a vertical moving distance of 300 mm, and (B) magnitudes of vibration in the three phases

X – frequency; *Y* – vertical acceleration magnitude

https://doi.org/10.17221/53/2023-RAE

distances of 50, 70, and 90 mm. A fast Fourier transform on the vibration acceleration signal of each measure using the MATLAB program to obtain the amplitude and frequency of acceleration is shown in Figure 8B. The vibration frequency over the total movement time was 8.5–11 Hz for all results. The RMS values of the amplitude vibration ranged from 0.166 to 0.597 mm.

Effect of the parameter pattern. Tables 1–3 shows the results of the vibration amplitude experiments using the harvester model and testing the parameters of time ratio, total movement time,

Table 1. Vibration amplitudes in 1st, 2nd, and 3rd phases for vertical moving distance of 200 mm

Parameter	Final phase distance	Total moving time	Time ratio	Vibration amplitude			Average vibration amplitude
			(T_1/T_2)	1st phase	2nd phase	3rd phase	
	(mm)	(s)		(mm)			
Vertical moving distance (200 mm)	50	1.50	1.50	0.899	0.707	0.797	0.589
			1.00	0.923	0.710	0.132	0.324
			0.75	0.841	0.600	0.240	0.439
		2.00	1.50	0.855	0.177	0.548	0.295
			1.00	0.877	0.707	0.436	0.279
			0.75	0.963	0.371	0.368	0.358
		2.50	1.50	0.710	0.267	0.339	0.224
			1.00	0.741	0.271	0.312	0.318
			0.75	0.819	0.366	0.277	0.418
	70	1.50	1.50	0.880	0.338	0.793	0.408
			1.00	0.867	0.612	0.816	0.401
			0.75	0.983	0.721	0.728	0.543
		2.00	1.50	0.632	0.214	0.655	0.215
			1.00	0.713	0.290	0.672	0.341
			0.75	0.906	0.520	0.312	0.374
		2.50	1.50	0.622	0.117	0.467	0.166
			1.00	0.669	0.231	0.398	0.192
			0.75	0.805	0.210	0.356	0.274
	90	1.50	1.50	0.707	0.204	0.790	0.338
			1.00	0.941	0.257	0.504	0.421
			0.75	1.124	0.370	0.664	0.460
		2.00	1.50	0.651	0.135	0.618	0.310
			1.00	0.701	0.182	0.608	0.205
			0.75	0.644	0.181	0.527	0.282
		2.50	1.50	0.587	0.188	0.354	0.168
			1.00	0.627	0.169	0.325	0.216
			0.75	0.799	0.042	0.394	0.193
Final phase distance	50	–	–	0.847[a]	0.464[c]	0.383[a]	0.361[c]
	70	–	–	0.786[a]	0.361[b]	0.577[b]	0.324[b]
	90	–	–	0.753[a]	0.192[a]	0.532[b]	0.288[a]
Time ratio	–	–	1.50	0.727[a]	0.261[a]	0.596[b]	0.302[a]
	–	–	1.00	0.784[a, b]	0.381[b]	0.467[a]	0.299[a]
	–	–	0.75	0.776[b]	0.376[b]	0.429[a]	0.371[b]
Total mov. time	–	1.50	–	0.907[b]	0.502[c]	0.607[c]	0.436[c]
	–	2.00	–	0.771[a]	0.309[b]	0.527[b]	0.296[b]
	–	2.50	–	0.709[a]	0.207[a]	0.358[a]	0.241[a]

[a, b] Letters in upper index indicates significant difference at 5% level; T_1 – the time of the first step movement; T_2 – the time of the final movement distance; D_f – final phase distance

https://doi.org/10.17221/53/2023-RAE

Table 2. Vibration amplitudes in 1st, 2nd, and 3rd phases for vertical moving distance of 250 mm

Parameter	Final phase distance	Total moving time	Time ratio	Vibration amplitude			Average vibration amplitude
			(T_1/T_2)	1st phase	2nd phase	3rd phase	
	(mm)	(s)		(mm)	(mm)	(mm)	(mm)
Vertical moving distance (200 mm)	50	1.50	1.50	1.018	0.635	0.517	0.328
			1.00	1.005	0.737	0.649	0.453
			0.75	0.932	0.797	0.451	0.417
		2.00	1.50	1.205	0.817	0.612	0.439
			1.00	0.930	0.845	0.528	0.520
			0.75	1.131	0.884	0.310	0.594
		2.50	1.50	0.790	0.822	0.338	0.318
			1.00	0.784	0.669	0.571	0.464
			0.75	1.031	0.742	0.372	0.449
	70	1.50	1.50	0.921	0.601	0.603	0.520
			1.00	0.987	0.757	0.673	0.503
			0.75	0.929	0.576	0.825	0.494
		2.00	1.50	0.894	0.231	0.643	0.339
			1.00	1.080	0.575	0.773	0.597
			0.75	0.738	0.592	0.601	0.481
		2.50	1.50	0.790	0.116	0.642	0.307
			1.00	0.828	0.611	0.267	0.405
			0.75	0.941	0.342	0.357	0.442
	90	1.50	1.50	0.898	0.160	0.882	0.479
			1.00	0.993	0.500	1.093	0.589
			0.75	1.033	0.762	0.859	0.507
		2.00	1.50	0.895	0.172	0.628	0.386
			1.00	0.887	0.442	0.729	0.566
			0.75	0.791	0.605	0.831	0.462
		2.50	1.50	0.821	0.199	0.808	0.245
			1.00	0.784	0.175	0.619	0.248
			0.75	0.949	0.562	0.445	0.384
Final phase distance	50	–	–	0.981a	0.772^{b}	0.483^{a}	0.442^{a}
	70	–	–	0.901^{a}	0.489^{a}	0.598^{a}	0.454^{a}
	90	–	–	0.895^{a}	0.398^{a}	0.766^{b}	0.430^{a}
Time ratio	–	–	1.50	0.915^{a}	0.417^{a}	0.630^{a}	0.373^{a}
	–	–	1.00	0.920^{a}	0.590^{b}	0.656^{a}	0.483^{b}
	–	–	0.75	0.942^{a}	0.651^{b}	0.561^{a}	0.470^{b}
Total mov. time	–	1.50	–	0.968^{b}	0.614^{b}	0.728^{b}	0.476^{b}
	–	2.00	–	$0.949^{a, b}$	0.574^{b}	0.628^{b}	0.487^{b}
	–	2.50	–	0.858^{a}	0.471^{a}	0.491^{a}	0.362^{a}

[a, b] Letters in upper index indicates significant difference at 5% level; T_1 – the time of the first step movement; T_2 – the time of the final movement distance; D_f – final phase distance

and final phase distance variables for three ranges of vertical movement (200, 250, and 300 mm). There was a significant effect of the final movement distance on the vibration amplitude in the 2nd and 3rd wave phases. An increase in the final movement distance from 5 to 9 cm reduced the vibration amplitude in the 2nd wave phase from 0.464 to 0.192, 0.772 to 0.398, and 0.772 to 0.579 mm in the vertical movement distances of 200, 250, and 300 mm, respectively. However, the vibration amplitude in the 3rd phase reversibly increased from 0.383 to 0.577, 0.483 to 0.766, and 0.382 to 0.551 mm, respectively.

https://doi.org/10.17221/53/2023-RAE

Table 3. Vibration amplitudes in 1st, 2nd, and 3rd phases for vertical moving distance of 300 mm

Parameter	Final phase distance	Total moving time	Time ratio	Vibration amplitude			Average vibration amplitude
			(T_1/T_2)	1st phase	2nd phase	3rd phase	
	(mm)	(s)		(mm)	(mm)	(mm)	(mm)
Vertical moving distance (200 mm)	50	1.50	1.50	0.881	0.769	0.450	0.399
			1.00	1.194	0.992	0.437	0.503
			0.75	1.125	0.985	0.482	0.558
		2.00	1.50	0.962	0.506	0.417	0.376
			1.00	1.079	0.804	0.620	0.377
			0.75	0.744	0.715	0.301	0.374
		2.50	1.50	0.862	0.522	0.330	0.276
			1.00	1.160	0.826	0.241	0.396
			0.75	1.104	0.810	0.162	0.356
	70	1.50	1.50	0.964	0.575	0.879	0.355
			1.00	1.272	0.552	0.895	0.498
			0.75	1.373	1.079	0.456	0.513
		2.00	1.50	0.910	0.576	0.518	0.315
			1.00	1.051	0.704	0.276	0.335
			0.75	0.975	0.707	0.324	0.387
		2.50	1.50	0.749	0.601	0.506	0.308
			1.00	0.879	0.397	0.324	0.320
			0.75	1.133	0.642	0.220	0.361
	90	1.50	1.50	1.045	0.709	0.897	0.366
			1.00	1.034	0.885	0.593	0.374
			0.75	1.060	0.598	0.534	0.432
		2.00	1.50	0.801	0.550	0.902	0.406
			1.00	1.045	0.541	0.543	0.416
			0.75	1.167	0.532	0.311	0.313
		2.50	1.50	0.959	0.497	0.420	0.233
			1.00	0.967	0.511	0.376	0.333
			0.75	0.982	0.384	0.386	0.336
Final phase distance	50	–	–	1.012[a]	0.772[b]	0.483[a]	0.442[a]
	70	–	–	1.034[a]	0.648[a]	0.489[b]	0.377[a,b]
	90	–	–	1.007[a]	0.579[a]	0.551[b]	0.356[a]
Time ratio	–	–	1.50	0.904[a]	0.589[a]	0.591[c]	0.337[a]
	–	–	1.00	1.076[b]	0.690[b]	0.478[b]	0.395[b]
	–	–	0.75	1.074[b]	0.717[b]	0.353[a]	0.403[b]
Total mov. time	–	1.50	–	1.105[b]	0.794[b]	0.625[c]	0.444[c]
	–	2.00	–	0.970[a]	0.626[a]	0.468[b]	0.366[b]
	–	2.50	–	0.977[a]	0.577[a]	0.330[a]	0.324[a]

[a, b] Letters in upper index indicates significant difference at 5% level; T_1 – the time of the first step movement; T_2 – the time of the final movement distance; D_f – final phase distance

The reduced difference in speed at starting and entering the longer final movement distance may have distributed the reduction of vibration in the 2nd wave phase and vice–versa in the 3rd wave phase since greater extended final movement allowed for a higher speed in the stop stage.

The final movement distance did not significantly affect the vibration amplitude in the 1st wave phase; when increasing the final phase distance (50, 70, and 90 mm), the average vibration amplitudes in the 1st wave phase for the three vertical movement distances were 0.795, 0.926, and 1.002 mm, respec-

https://doi.org/10.17221/53/2023-RAE

tively. However, the final movement distance affected the average vibration amplitude of the whole wavelength, with a more extended period of the final movement reducing the average value of the whole vibration amplitude. Considering the effects on the three–wave phases, managing the final phase distance could help make the vibration amplitude more uniform. The final movement distance should not be over one–half of the vertical moving distance; otherwise, the higher deceleration in the stopping stage causes a greater vibration amplitude in the 3rd phase. The time ratio influenced the vibration amplitude because an increase in the time ratio under the same total movement time significantly reduced the vibration amplitude in the 2nd wave phase. Operating under an increasing time ratio from 0.75 to 1.50 for vertical movement distances of 200, 250, and 300 mm decreased the average vibration amplitudes in the 2nd wave phase from 0.376 to 0.261, from 0.651 to 0.417, and from 0.717 to 0.589 mm, respectively. The higher the time ratio, the lower the speed obtained at the starting point, decreasing acceleration and reducing the difference between the start speed and the final speed, resulting in a lower vibration amplitude in the 2nd phase for the same final phase distance. However, there was a significantly increased effect on the vibration amplitude in the 3rd phase due to a higher declaration value in the stopping stage. When the header model operated under a time ratio increasing from 0.75 to 1.50 in the vertical moving distance of 200, 250, and 300 mm, the average vibration amplitudes decreased from 0.370 to 0.299, from 0.470 to 0.373, and from 0.403 to 0.337 mm, respectively, over the total movement time; analyzing the interaction between the time ratio and the final phase distance in the vertical movement distance of 200, 250, and 300 mm affected vibration amplitude. With an increase in both the time ratio (from 0.75 to 1.50) and in the final movement distance (from 50 to 90 mm), the average vibration amplitude was reduced in the range 0.487 to 0.263 mm, with 1.144 to 0.648 mm in the 1st wave phase and 0.874 to 0.176 mm in the 2nd wave phase but this increased from 0.295 to 0.772 mm for the 3rd wave phase for the vertical movement distance from 200 to 300 mm. These results suggested that manipulating two parameters could manage the vibration's amplitude and help keep it consistent over the entire range of motion. The control system should keep the time ratio and the final movement distance minimal to optimize the relationship between the excitation parameters to minimize the vibration amplitude in the 3rd wave phase. On the other hand, to reduce the vibration amplitude in the 1st and 2nd wave phases, the system must control the start speed and final speed by more closely managing the time ratio and the total movement time.

The total movement time also significantly affected the vibration amplitude. The experimental results showed that increasing the total movement time from 1.5 to 2.5 s for vertical movement distances of 200, 250, and 300 mm significantly reduced the

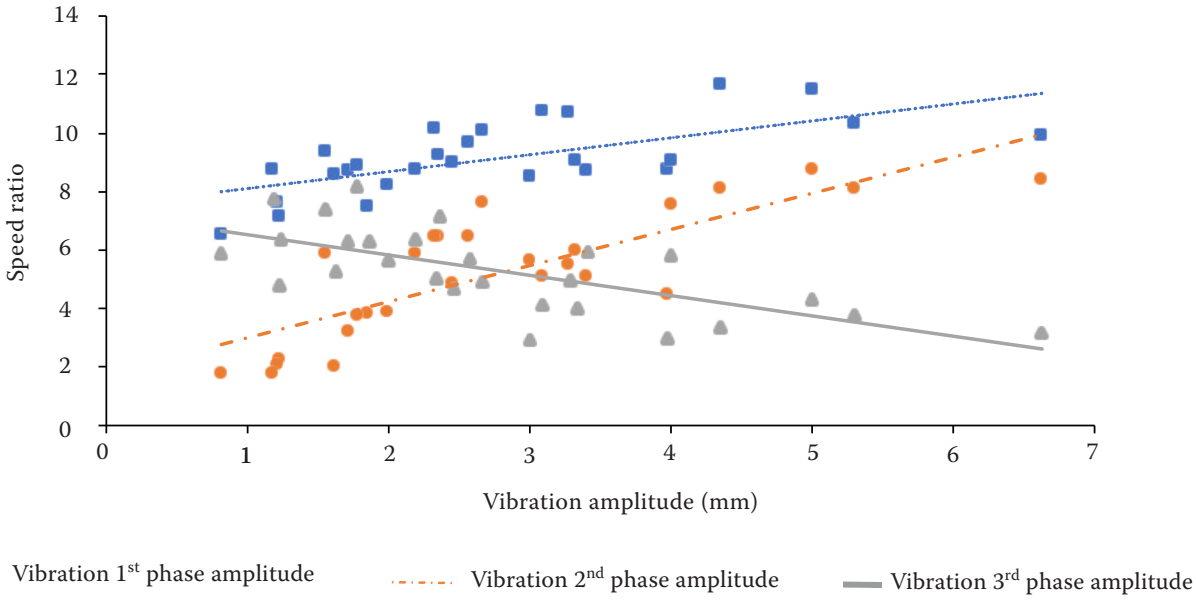

Figure 9. Correlations between speed ratio and vibration amplitude

https://doi.org/10.17221/53/2023-RAE

vibration amplitude in all wave phases. The vibration amplitude in the 1st, 2nd, and 3rd wave phases decreased from 0.197 to 0.110 mm, 0.295 to 0.143 mm, and 0.295 to 0.237 mm, respectively, with the vibration amplitude in the second wave phase having the most significant reduction. However, the total movement time must be carefully considered in conjunction with the travel speed in rice harvesting situations in a field to avoid incorrect rice cutting in the changing area between lodging and standing rice.

Figure 9 shows the effect of the speed ratio on the vibration amplitude in the 1st, 2nd, and 3rd wave phases. The vibration amplitude had a positive linear relationship with the speed ratio in the 1st and 2nd wave phases but a negative linear relationship in the 3rd wave phase. Increasing the speed ratio with the same total movement time produced a greater difference between the start and final speeds, resulting in increased vibration amplitude in the 2nd phase. On the other hand, this reduced vibration amplitude in the 3rd phase. Therefore, selecting the appropriate speed ratio could help to lower the vibration amplitude and make it more consistent. For a control header with a vertical movement distance of 200 mm or less in the field, setting the speed ratio to 1 can help reduce the vibration amplitude in the 1st and 2nd wave phases. However, a higher start speed is necessary for a vertical movement distance of 250 mm or more to make the corresponding response fast enough to cut the rice accurately.

CONCLUSION

The natural frequency of the harvester model was in the range of 8.5–11 Hz, and the root mean square of the vibration amplitude was in the range of 0.166–0.597 mm.

The harvester header models investigated parameters (time ratio, total movement time, and final movement distance) significantly influenced the vibration amplitude.

The vibration amplitude was affected by the interaction of two parameters (time ratio and final phase distance) for all vertical movement distances (200, 250, and 300 mm). Increases in the time ratio and the final phase distance decreased the vibration amplitude in the 1st and 2nd phases.

Using the minimum time ratio and final phase distance resulted in the minimum vibration amplitude in the 3rd phase. The closer the start speed and final speed, the smaller the vibration amplitude in the 1st and 2nd phases.

An increase in the total movement time significantly lowered the vibration amplitude.

The speed ratio increased the vibration amplitude for the 1st and 2nd wave phases but reduced it for the 3rd wave phase.

When operating at a vertical movement distance of 200–300 mm, a time ratio of 0.75 and a final phase distance of 50 mm are recommended. These adjustments effectively reduced the vibration amplitude in the 3rd wave phases, resulting in more accurate rice cutting.

REFERENCES

An X., Li Z., Zude–Sasse M., Tchuenbou–Magaia F., Yang Y. (2020): Characterization of textural failure mechanics of strawberry fruit. Journal of Food Engineering, 282: 1–10.

Baerdemaeker J.D., Saeys W. (2013): Advanced control of combine harvesters. 4th IFAC Conference on Modelling and Control in Agriculture. Horticulture and Post Harvest Industry. Espoo, Finland, Aug 27–30, 2013: 46: 1–5.

Buscarello R.T. (1994): Practical Solutions of Machinery and Maintenance Vibration Problems. 5th Ed. Update International, Denver: 265.

Chen S., Zhou Y., Tang Z., Lu S. (2020): Modal vibration response of rice combine harvester frame under multi–source excitation. Biosystems Engineering, 194: 177–195.

Chinsuwan W., Pongjan N., Chuan–Udom S., Phayom W. (2003): Effects of feedrate and threshing speed on performance of axial flow rice thresher. TSAE Journal, 10: 9–14.

Chuan–Udom S. (2010): Development of a cutter bar driver for reduction of vibration for a rice combine harvester. KKU Research Journal, 15: 572–580.

Ebrahimi R., Esfahanian M., Ziaei–Rad S. (2013): Vibration modeling and modification of cutting platform in a harvest combine by means of operational modal analysis (OMA). Measurement, 46: 3959–3967.

Fukushima T., Inoue E., Mitsuoka M., Okayasu T., Sato K. (2012): Collision vibration characteristics with interspace in knife driving system of combine harvester. Engineering in Agriculture, Environment and Food, 5: 115–120

Glancey J. (1997): Analysis of header loss from pod stripper combines in green peas. Journal of Agricultural Engineering Research, 68:1–10.

Gao Z., Xu L., Li Y., Wang Y., Sun P. (2017): Vibration measure and analysis of crawler–type rice and wheat combine harvester in field harvesting condition. Transactions of the Chinese Society of Agricultural Engineering, 33: 48–55.

https://doi.org/10.17221/53/2023-RAE

Huang D., Zhou S., Litak G. (2019): Analytical analysis of the vibrational tri–stable energy harvester with a RL resonant circuit. Nonlinear Dynamics, 97: 663–677.

Junsiri C., Chinsuwan W. (2009): Prediction equations for header losses of combine harvesters when harvesting Thai Hom Mali rice. Songklanakarin Journal of Science and Technology, 31: 613–620.

Lai Z.N., Yang S., Wu P., Wu D. (2018): Speed–throttling combined optimization for high reliability in parallel centrifugal pump system. Journal of Drainage and Irrigation Machinery Engineering, 36: 1205–1210 and 1221.

Lopes G.T., Magalhães P.S.G., Nóbrega E.G.O. (2002): AE–automation and engineering technologies: Optimal header height control system for combine harvesters. Biosystems Engineering, 81: 261–272.

Lashgari M., Hossein M., Omid M., Alimardani R., Mohtasebi S.S. (2008): Qualitative analysis of wheat grain damage during harvesting with john deere combine harvester. International Journal of Agriculture and Biology, 10: 201–204.

Ni Y., Jin C., Chen M., Yuan W., Qian Z., Yang T., Cai Z. (2021): Computational model and adjustment system of header height of soybean harvesters based on soil–machine system. Computers and Electronics in Agriculture, 183: 105907.

Parihar D.S., Narang M.K., Dogra B., Prakash A., Mahadik A. (2023): Rice residue burning in Northern India: An assessment of environmental concerns and potential solutions– a review. Environmental Research Communications, 5: 062001.

Quick G. R., Buchele W. F. (1974): Reducing combine gathering losses in soybeans. Transactions of the ASAE, 17: 1123–1129.

Ruan M., Jiang H., Zhou H., Ye J., Hu J. (2022): Design and test of automatic control system for header height of combine harvester. INMATEH Agricultural Engineering, 68: 569–578.

Tang Z., Zhang H., Zhou Y., Li Y. (2019a): Mutual interference and coupling response of multicylinder vibration among combine harvester co–frame. Shock and Vibration, 2019: 1584391.

Tang Z., Zhang H., Zhou Y., Li Y. (2019): Effects of stem cutting in rice harvesting by combine harvester front header vibration. Advances in Materials Science and Engineering, 2019: 6834269.

Xie Y., Alleyne A., Greer A., Deneault D. (2010): Header height control of a combine harvester system. The American Society of Mechanical Engineers. 2010 Dynamic Systems and Control Conference. Cambridge, Sept 12–15, 2010: 7–14.

Wang G., Su R. (2021): Research on ground profiling control of combine harvester based on the symmetric algorithm. Journal of Physics: Conference Series, 1827: 012211.

Xie Y., Alleyne A. (2014): Two degree of freedom control synthesis with applications to agricultural systems. Journal of Dynamic Systems, Measurement, and Control, 136: 051006.

Xia C., Wang L., Chung B.–K., Lee J.–M. (2015): *In situ* 3D segmentation of individual plant leaves using a RGB–D camera for agricultural automation. Sensors, 15: 20463–20479.

Yang R., Wang Z., Shang S., Zhang J., Qing Y., Zha X. (2022): The design and experimentation of EVPIVS–PID harvesters' header height control system based on sensor ground profiling monitoring. Agriculture, 12: 282.

Yong L., Yang X., Ming W., Da L., Yi C., Ya L. (2018): Design and test of the adaptive height adjustment system for header of the combine–harvester. Journal of Hunan Agricultural University, 44: 326–329.

Zhu J., Yin W.Q., Xie B. (2012): Application of embedded electro–hydraulic proportional control system in height control of combine harvester header. Hydraulics & Pneumatics, 44: 83–86.

Received: May 26, 2023
Accepted: January 16, 2024
Published online: June 26, 2024